


Article

Effect of Cerium (IV) Oxide Particle Size on Polydimethylsiloxane Polymer to Form Flexible Materials against Ionizing Radiation

Haifa M. Almutairi¹, Wafa M. Al-Saleh^{2,3} , Mohammad Ibrahim Abualsayed^{4,5}  and Mohamed Elsafi^{6,*} 

¹ Medical Physics Department, Umm Al-Qura University, Prince Sultan Bin Abdul-Aziz Road, Mecca P.O. Box 715, Saudi Arabia; hmutayri@uqu.edu.sa

² College of Science and Health Professions, King Saud bin Abdulaziz University for Health Sciences, Al-Ahsa P.O. Box 6664, Saudi Arabia; salehw@ksau-hs.edu.sa

³ King Abdullah International Medical Research Center, Al-Ahsa P.O. Box 3660, Saudi Arabia

⁴ Department of Physics, Faculty of Science, Isra University, Amman 11622, Jordan

⁵ Physics Department, Faculty of Science, Universiti Teknologi Malaysia, Skudai 81310, Malaysia

⁶ Physics Department, Faculty of Science, Alexandria University, Alexandria 21511, Egypt

* Correspondence: mohamedelsafi68@gmail.com

Abstract: This study aims to investigate the impact of CeO₂ content and particle size on the radiation shielding abilities of polydimethylsiloxane, also known as silicon rubber (SR). We prepared different SR samples with 10, 30, and 50% of micro and nano CeO₂ and we measured the linear attenuation coefficient (LAC) for these samples. We found that the LAC of the SR increases by increasing the CeO₂ and all prepared SR samples had higher LACs than the pure SR. We examined the effect of the size of the particles on the LAC and the results demonstrated that the LAC for nano CeO₂ is higher than that of micro CeO₂. We investigated the half value layer (HVL) for the prepared SR samples and the results revealed that the SR with 10% micro CeO₂ had a greater HVL than the SR with 10% nano CeO₂. The HVL results demonstrated that the SR containing nanoparticles had higher attenuation effectiveness than the SR with micro CeO₂. We also prepared SR samples containing CeO₂ in both sizes (i.e., micro and nano) and we found that the HVL of the SR containing both sizes was lower than the HVL of the SR with nano CeO₂. The radiation protection efficiency (RPE) at 0.059 MeV for the SR with 10% micro and nano CeO₂ was 94.2 and 95.6%, respectively, while the RPE of SR containing both sizes (5% micro CeO₂ + 5% nano CeO₂) was 96.1% at the same energy. The RPE results also indicated that the attenuation ability was improved when utilizing the micro and nano CeO₂ as opposed to the micro CeO₂ or nano CeO₂ at 0.662, 1.173, and 1.333 MeV.

Keywords: polydimethylsiloxane; CeO₂-nanoparticles; radiation shielding; attenuation coefficient



Citation: Almutairi, H.M.; Al-Saleh, W.M.; Abualsayed, M.I.; Elsafi, M. Effect of Cerium (IV) Oxide Particle Size on Polydimethylsiloxane Polymer to Form Flexible Materials against Ionizing Radiation. *Polymers* **2023**, *15*, 2883. <https://doi.org/10.3390/polym15132883>

Academic Editor: Chi-Hui Tsou

Received: 16 May 2023

Revised: 15 June 2023

Accepted: 27 June 2023

Published: 29 June 2023



Copyright: © 2023 by the authors. Licensee MDPI, Basel, Switzerland. This article is an open access article distributed under the terms and conditions of the Creative Commons Attribution (CC BY) license (<https://creativecommons.org/licenses/by/4.0/>).

1. Introduction

Ionizing radiation can leave permanent damage on the human body as a result of the high energy of the photons that it consists of. Radiation, on the other hand, is of tremendous use in a variety of fields, including medicine, scientific research, industry, and agriculture. To ensure that the potential risks of radiation are not outweighed by its beneficial applications, appropriate precautions must be taken to reduce the negative effects of radiation as much as possible. In order to achieve this goal, the concepts of time (which include reducing the total amount of time spent in contact with radiation), distance (which involves maximizing the distance from the origin of the radiation), and the application of radiation shields are utilized [1–3]. A radiation shield is any substance that is employed to attenuate radiation and acts as a barrier between the source of the radiation and a person who is being protected by the shield. When selecting a shield to serve a particular function, numerous variables are taken into consideration in order to decide on the material that will be ideal for performing that function. For example, concrete has been shown to be

quite efficient against X-rays and neutrons, making it an excellent material to employ as a liner for the walls of rooms containing machinery that utilizes radiation. In certain situations, concrete can be an excellent barrier; however, the material's drawbacks, such as its tendency to crack and that it is unable to be moved, make it ineffective for a variety of other applications [4,5]. The most common radiation shielding material is lead, as well as products containing lead, due to its dense nature, inexpensive price, and superior shielding properties. Lead could seem like the perfect material for a shield, but its toxicity toward both people and the environment makes it less useful. The need for lead alternatives has increased recently, particularly in the medical industry, in an effort to curtail and eventually stop the use of lead as a shield. Glass is an additional substance that is employed as a radiation barrier. Glass has the special quality of being transparent as well as having a variety of compositions and being simple to manufacture [6–11].

Polymers represent a potentially attractive and acceptable option as shielding materials due to their exceptional chemical, physical, electrical, and radiation resistance capabilities, along with their flexibility, light weight, and durability. In addition, polymers can be efficiently doped with considerable quantities of high atomic number elements to form their composites, which are superior radiation shields [12]. Although polymers normally perform less well at radiation shielding than metals, their efficiency can be greatly increased by adding more radiation shielding chemicals to the polymer matrix [13]. Recently, polymer composites have drawn interest as viable, lightweight replacements for metal radiation protective technologies [14–16]. Polymers are multipurpose substances that are simple to mold for the intended applications. A single polymer cannot meet the criteria for technological usage in this area; hence, a number of factors must be taken into account. As a result, polymer composites have garnered interest on a global level.

Silicon rubber is often regarded as one of the polymers with a high degree of flexibility. This characteristic has a wide range of potential uses, particularly in the medical industry. As it can protect the body during a radiology evaluation, it must be enhanced with materials that have a higher density and can absorb photons. This will allow it to better serve its purpose [17,18]. Additives, such as heavy metal oxides and nanoparticles, may be incorporated into the polymers in order to enhance the rubbers' capacity to shield electromagnetic radiation [19–21]. Typically, a bulk matrix and nano dimensions solid phase materials are combined to form nanocomposite materials. The nanocomposites made from polymers have benefits in terms of dimensional variation and flexibility. Radiation shielding is one application where polymers, composites, and polymeric nanocomposites are crucial. Materials made of polymer composites or nanocomposites have been used in a variety of industries, including in satellites, aerospace, nuclear reactors, etc. In any case, polymer composites have emerged as excellent prospects for the development of materials capable of attenuating photons or other types of particle radiation [22].

The macromolecular state around nanoparticles changes as a result of the high surface-to-volume ratio that distinguishes nanoparticles from other materials. The properties of the polymer are improved by the inclusion of nanoparticles, including improved elastic stiffness, strength, reduced gas permeability, and radiation shielding effectiveness [23]. Due to its excellent qualities and distinctive features, cerium oxide (CeO_2) is attracting attention as a potential radiation shielding material. CeO_2 is able to attenuate gamma photons because of its high atomic number. Radiation can be efficiently scattered and absorbed by the thick structure of CeO_2 , which reduces the amount of radiation that passes through the material. Moreover, CeO_2 is ideal for long-term protection purposes due to its outstanding stability and radiation damage resistance. Furthermore, CeO_2 is simply manufactured in a variety of shapes, such as bulk and nano-sized materials as well as thin films, providing versatility in the development and utilization of radiation shielding technologies [24,25]. Further research on CeO_2 's potential as a protective material is required in the fields of radiation protection and nuclear security. For this reason, we prepared silicon rubber with micro and nano CeO_2 and reported the radiation shielding properties of the prepared samples.

2. Materials and Method

We fabricated new flexible composites based on polydimethylsiloxane (this is a flexible polymer with interesting properties for biomedical applications, including physiological indifference, excellent resistance to biodegradation, biocompatibility, chemical stability, gas permeability, good mechanical properties, and excellent optical transparency) as a matrix material and cerium oxide (CeO_2) with different particle sizes. The polydimethylsiloxane polymer was supplied from Alhuda Chemical in Egypt. The CeO_2 was separated into 2 sizes, micro and nano. The average size of micro particles was $10 \mu\text{m}$, supplied by Algamhoria Chemicals Company, while the CeO_2 nanoparticle average size was $20 \pm 3 \text{ nm}$, supplied from Nano Gate Company. The micro and nano CeO_2 were supplied from Nano Gate Company. The average size of micro CeO_2 was checked using an SEM scan as shown in Figure 1a, while the nano CeO_2 was scanned by TEM analysis as shown in Figure 1b.

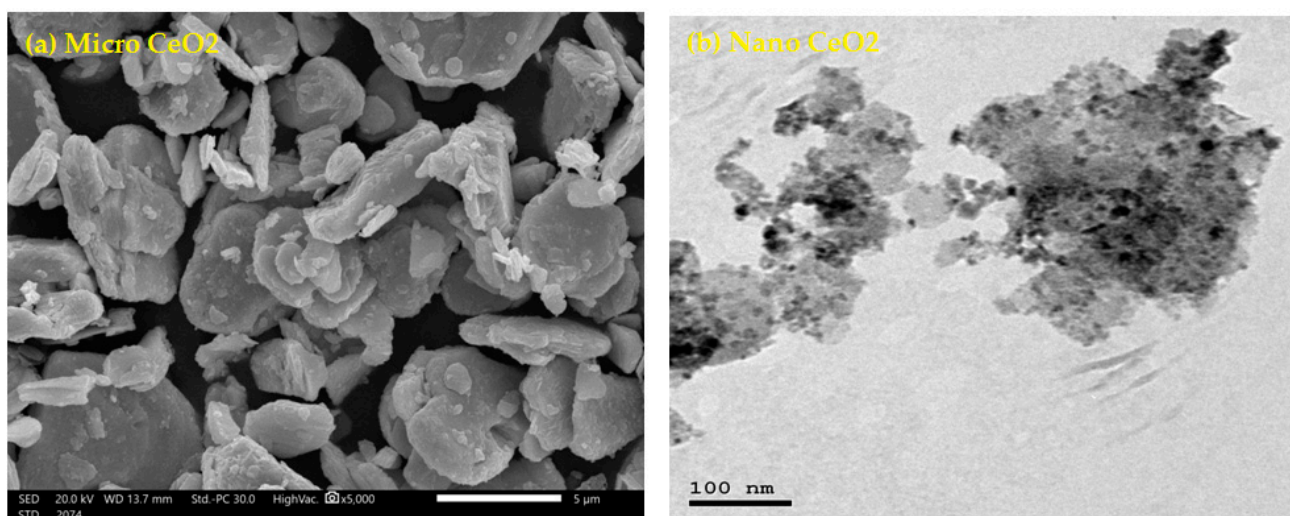


Figure 1. SEM and TEM images of micro and nano CeO_2 , respectively. (a) SEM of micro CeO_2 and (b) TEM of nano CeO_2 .

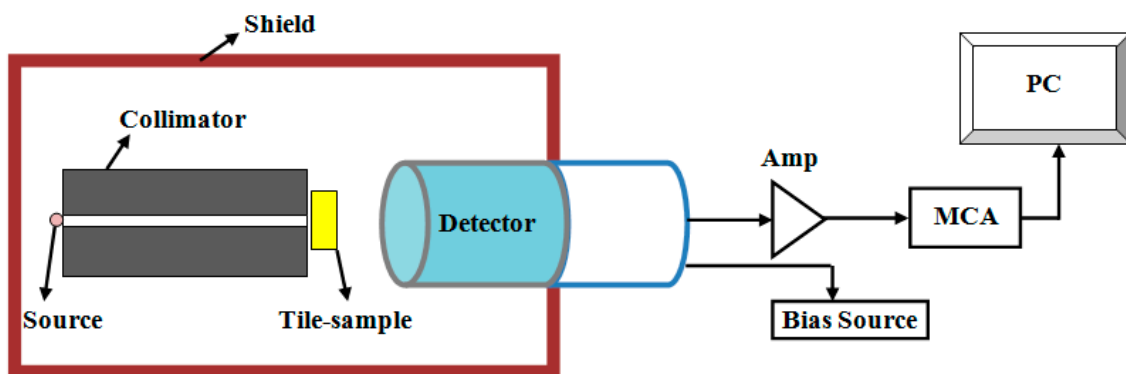
After collecting the basic materials, we prepared 10 different flexible SR samples, and each sample had different thicknesses (0.98, 1.35 and 2 cm). The weight percentage (%) ratio of SR to hardener was 95:5 in all preparations, and percentages of micro, nano, and 0.5 micro + 0.5 nano CeO_2 are reported in Table 1. To obtain a homogeneous composite, the compounds were mixed with a hand mixer for a sufficient period equal to a quarter of an hour at room temperature, then placed in plastic crucibles of different thicknesses and left for 24 h until they became cohesive and flexible. The density of composites was measured and reported in Table 1 by evaluating the mass to volume ratio, where the mass was measured by 0.001 g sensitive electric balance and the volume measured by $\frac{4}{3}\pi r^3$, where r represents the radius of the SR composite [26].

The attenuation or absorption parameters of these composites and the experimental LAC cm^{-1} were determined. The main devices used in the experimental technique were the point gamma ray sources, lead collimator, and HPGe detector connected to liquid nitrogen as well as an electronic unit containing a high voltage, multichannel analyzer connected to a computer, as shown in Figure 2. The detector was calibrated to get the best geometry for the measurements, and the free sample intensity of present sources was measured (I_0). The sources were AM-241, Cs-137, and Co-60. Following this, the measurements were undertaken on an occupied SR sample to calculate the intensity (I) at a specific SR thickness (x). From these values, the experimental LAC can be calculated from the next relation [27–29]:

$$\text{LAC} = \frac{1}{t} \ln \frac{I_0}{I} \quad (1)$$

Table 1. Codes, compositions, and densities of the different fabricated fixable samples.

Sample Name	Sample Code	SR (wt%)	CeO ₂ Micro (wt%)	CeO ₂ Nano (wt%)	Density (g·cm ⁻³)
Pure SR	SR ₀	100	—	—	1.302 ± 0.006
SR with Micro CeO ₂	SR _{M10}	90	10		1.410 ± 0.011
	SR _{M30}	70	30		1.722 ± 0.010
	SR _{M50}	50	50		2.201 ± 0.009
SR with Nano CeO ₂	SR _{N10}	90		10	1.421 ± 0.010
	SR _{N30}	70		30	1.742 ± 0.007
	SR _{N50}	50		50	2.210 ± 0.008
SR with Micro and Nano CeO ₂	SR _{M5N5}	90	5	5	1.416 ± 0.009
	SR _{M15N15}	70	15	15	1.736 ± 0.007
	SR _{M25N25}	50	25	25	2.213 ± 0.022

**Figure 2.** The experimental setup in the LAC measurement.

To ensure the validity of the experimental values, the online Phy-X software was used to calculate the LAC of the pure SR composite. The Phy-X software can calculate the shielding values for photon energies between 0.015 MeV and 100 GeV for the molecular or elemental structure of any material [30]. The software accounts for the chemical makeup and density of the constituents while calculating these characteristics. Different shielding parameters, such as LAC, MFP, HVL, and TVL, can be calculated for each material. The relative deviation of 2 results is given by:

$$RD(\%) = \frac{LAC_{Phy-x} - LAC_{Exp}}{LAC_{Exp}} * 100 \quad (2)$$

The relative increase between the composites containing micro and nano CeO₂ (RI₁) and the relative increase between the composites containing micro and (0.5 micro + 0.5 nano) CeO₂ (RI₂) were calculated as below:

$$RI_1(\%) = \frac{LAC_{Nano} - LAC_{Micro}}{LAC_{Micro}} * 100 \quad (3)$$

$$RI_1(\%) = \frac{LAC_{0.5N+0.5M} - LAC_{Micro}}{LAC_{Micro}} * 100 \quad (4)$$

The half value layer, 10th value layer, and radiation protection efficiency, denoted by HVL, TVL, and RPE, respectively, are essential factors for the shielding material properties and can be expressed by the following laws [31,32]:

$$HVL = \frac{\ln(2)}{LAC} \quad (5)$$

$$\text{TVL} = \frac{1}{\text{LAC}} \quad (6)$$

$$\text{RPE, \%} = \left[1 - \frac{I}{I_0} \right] \times 100 \quad (7)$$

3. Results and Discussion

SEM morphologies of the SR_0 , SR_{M50} , SR_{N50} , and $\text{SR}_{\text{M25N25}}$ composites were performed to observe the distribution of CeO_2 size inside the silicon rubber, as shown in Figure 3. The results of the images show that the mixture of the micro and nano particles leads to a symmetrical and homogeneous distribution within the mixture, which reduces the voids between the silicon particles. This is evident in Figure 3d. The result of this good distribution makes the attenuation of the incident photons on the SR composite higher, which increases its shielding efficiency as shown below.

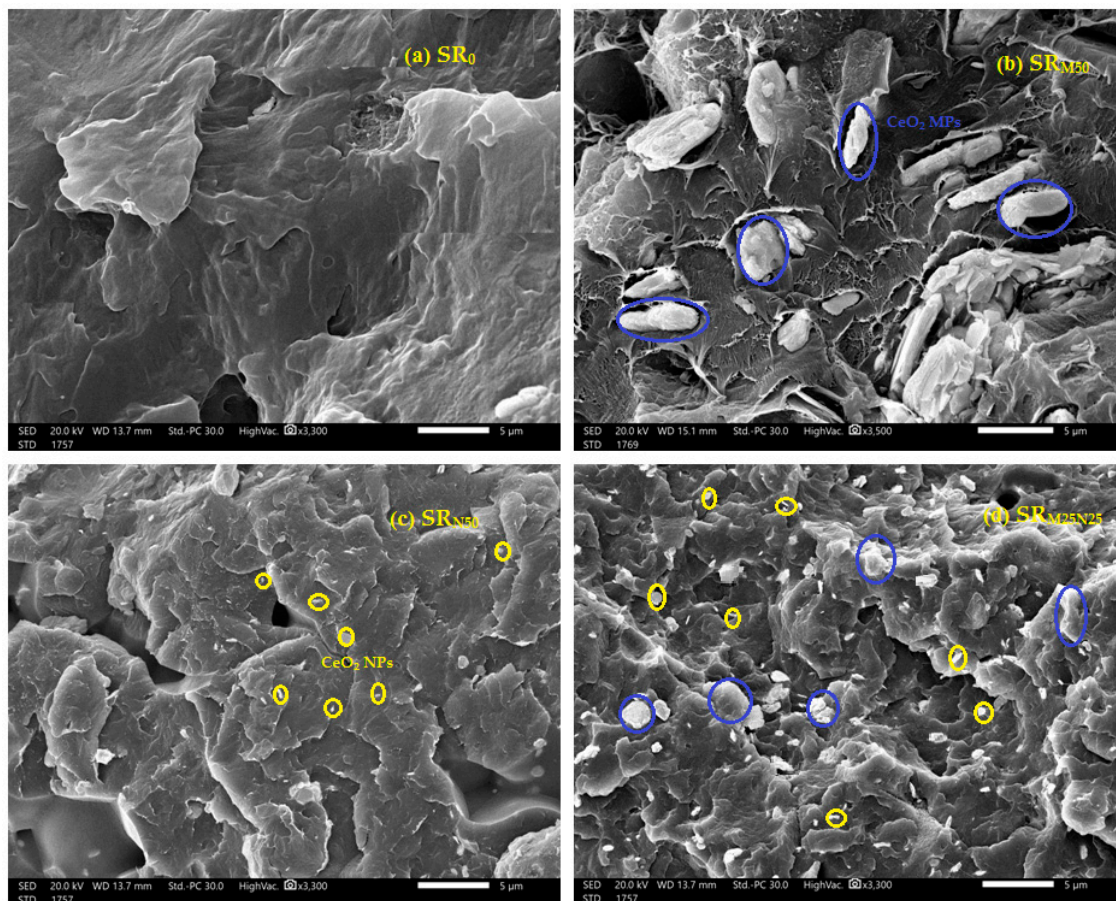


Figure 3. SEM images of the prepared fixable composites. (a) SR_0 , (b) SR_{M50} , (c) SR_{N50} , and (d) $\text{SR}_{\text{M25N25}}$.

The purpose of this work was to analyze the radiation shielding capabilities of the synthesized SR and to assess the effects of various CeO_2 contents, particle sizes (micro and nano) on the linear attenuation coefficient (LAC), and other related parameters. The first step is to test the accuracy in the setup used for the determination of the LAC for our samples. For this reason, we compared the experimental and Phy-X LAC for the pure SR samples. In Figure 4a, the LAC values determined by Phy-X are depicted in black squares, whereas the experimental LAC values are displayed in red circuits. Additionally, we display in Figure 4b the relative difference (R.D.) between the LACs for the pure SR

sample obtained through experimental and theoretical methods. The R.D. represents the precision of the setup of the experiments employed in this study to calculate the LAC for the other kinds of samples (SR with micro and nano CeO_2). The R.D. is minimal and falls within experimental uncertainty. Furthermore, as seen in Figure 3a, there is good agreement between the experimental and theoretical LACs, which shows that the experimental setup used in our work is appropriate for measuring the LAC of the SR with various CeO_2 concentrations.

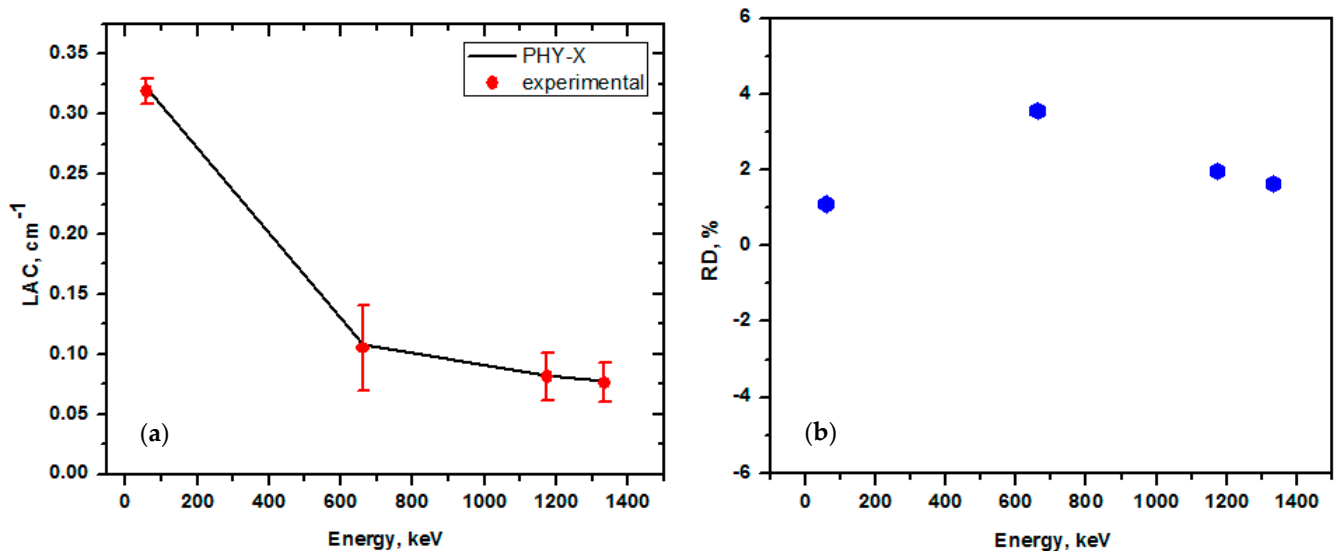


Figure 4. The experimental and theoretical LACs of the pure SR sample. (a) LAC and (b) relative deviation.

In Figure 5, we presented the LACs for the pure SR and for the SR with 10, 30, and 50% of micro and nano CeO_2 . It is evident that regardless of whether the CeO_2 is micro or nano, the LAC of the SR increases with increasing CeO_2 concentration. This is due to the inclusion of the high atomic number elements (i.e., Ce with $Z = 58$). The pure SR has a lower LAC than all other SRs with CeO_2 . Therefore, increasing the amount of bulk CeO_2 or NPs that are included within the SR can improve its ability to shield gamma photons. However, the speed at which the LAC increases is dependent on the energy of the photon that is being emitted. When CeO_2 is added, the LAC value is shown to increase considerably at low energies; however, at high energies, the LAC value just slightly increases when CeO_2 is added. This is due to the fact that the photoelectric effect is the most important process at low energy, and it is known that the cross section of this process highly depends on the atomic number of the materials. So, as we added CeO_2 , there was a notable increase in the LAC. However, at higher energies, the Compton scattering is the main photon–matter interaction process, and the cross section of this process has a weak dependence on the atomic number of the shielding materials, so we noticed a small increase in the LAC due to the addition of CeO_2 at higher energies. The following section considers nano CeO_2 and investigates how much the LAC increased for the lowest and highest measured energies.

The LAC for the pure SR at 0.059 MeV is 0.319 cm^{-1} , while the LAC values are 1.56, 4.90, and 10.12 cm^{-1} for the SR with 10, 30, and 50% nano CeO_2 . As a consequence of this finding, the LAC improved as a direct result of the addition of 50% nano CeO_2 to the SR. In the meantime, the values of the LAC for the pure SR, as well as the SR containing 10, 30, and 50% nano CeO_2 , were 0.076, 0.085, 0.101, and 0.125 cm^{-1} , respectively, when measured at 1.333 MeV. As a result, the LAC at high energies exhibits only a slight increase as a result of the inclusion of nano CeO_2 , as can be easily observed in the results shown in Figure 5.

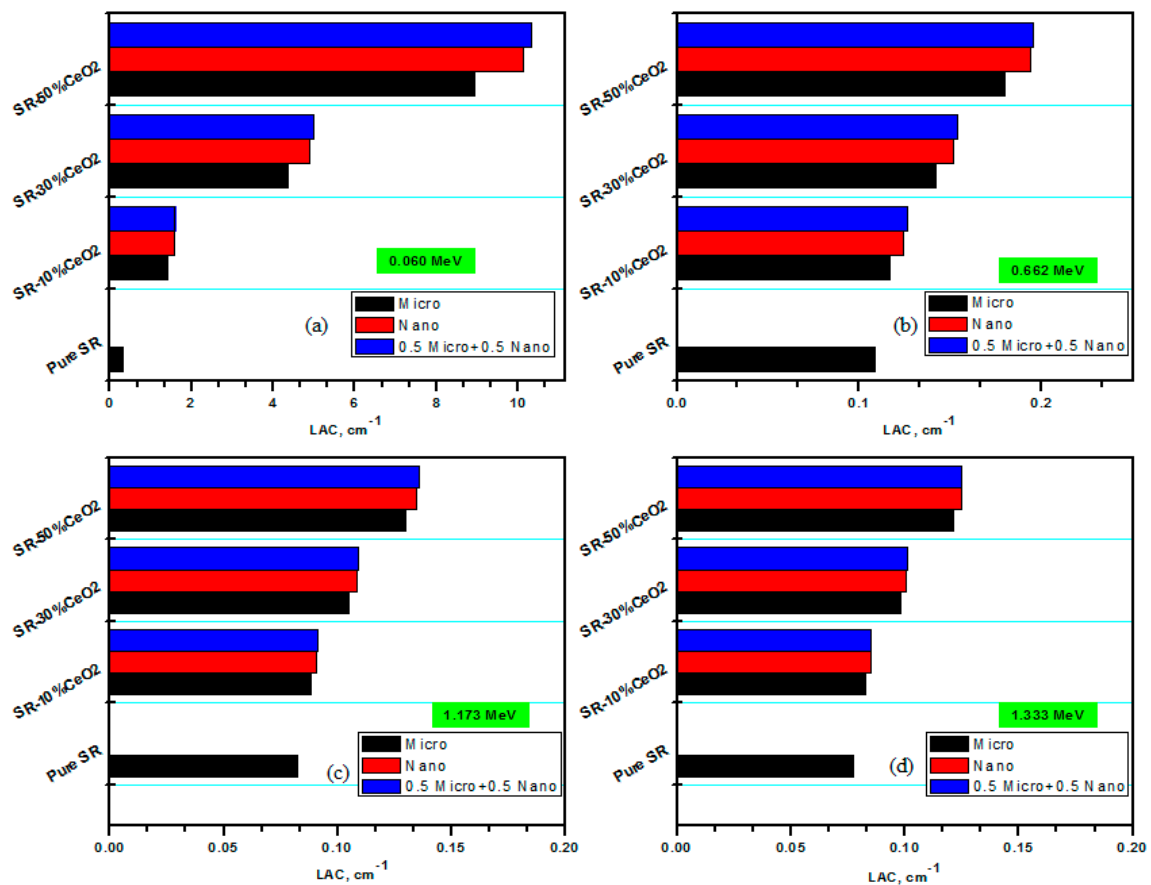


Figure 5. The LACs of different SR-CeO₂ composites at different energies. (a) at 0.060 MeV, (b) at 0.662 MeV, (c) at 1.173 MeV, and (d) at 1.333 MeV.

When the effect of the size of the particles on the LAC values is examined, it can be shown that the LACs for nano CeO₂ are higher than that of micro CeO₂, which appears as follows: (LAC) CeO₂-nano > (LAC) CeO₂-micro > (LAC)free CeO₂. The particle distribution in the SR is the reason why the LAC values for CeO₂ NPs are higher than those for micro CeO₂. The NPs lower size enables a more uniform distribution of particles inside the SR, increasing the surface to mass ratio and raising the likelihood that gamma rays will interact with the CeO₂ NPs. This is why the SR with NPs has superior attenuation capabilities than the SR with micro CeO₂. Similar observation was revealed by Cheewasukhanonta et al., who examined the impact of nano and micro Bi₂O₃ on the attenuation factors for certain glass systems [33].

We prepared new samples that contain 5% micro CeO₂ and 5 nano CeO₂, 15% micro CeO₂ and 15 nano CeO₂, and 25% micro CeO₂ and 25 nano CeO₂. We used the abbreviation 0.5 M–0.5 N for these samples. We aimed to check the radiation shielding effectiveness of these samples that contain CeO₂ in both sizes (i.e., micro and nano). Since the LACs for the nano CeO₂ samples are higher than those of micro CeO₂, we found that the LAC for the 0.5 M–0.5 N samples is higher than the LAC for the samples with nano CeO₂, as shown in Figure 5. There are a variety of reasons why the LAC of the sample with both micro and nano CeO₂ is higher than the LAC values for the samples with nano CeO₂. First, the presence of both micro- and nano-sized CeO₂ in the composite sample allows the SR to be more efficient at absorbing the incoming radiation. This enhancement can be attributed to the ability of different sized particles to interact with radiation from different energy ranges, leading to greater overall attenuation. Additionally, the distribution of particles within the composite sample may also cause this increase in LAC. Namely, the composite sample may have greater homogeneity compared to the sample with nano CeO₂ because of the

concentration of nanoparticles alongside the microparticles. This distribution of particles leads to more consistent attenuation of radiation across the samples.

The relative increase (RI, %) between the LAC values at each level of CeO₂ was calculated in order to better understand the difference between the shielding effectiveness of micro and nano CeO₂-SR (RI₁) as well as the difference between the shielding effectiveness of micro and 0.5 micro + 0.5 nano CeO₂-SR (RI₂) against gamma photons. The ratios for the SR with 10, 30, and 50% CeO₂ are displayed in a histogram in Figure 6. It is clear that as photon energy increases, the relative increase drops, highlighting how significantly CeO₂ influences the SR ability to attenuate radiation at low energies. Additionally, it is evident that 30% CeO₂ has a greater relative increase than 10% CeO₂. The maximum RI (%) was reported for 50% CeO₂ NPs at 0.059 MeV and is 31.10% and 15.30% for RI₁ and RI₂, respectively. Consequently, it can be stated that CeO₂ nanoparticles are a more promising material to use in the development of efficient shielding materials than the micro particles, while the combination of both sizes of CeO₂ gave better shielding development and a lower cost.

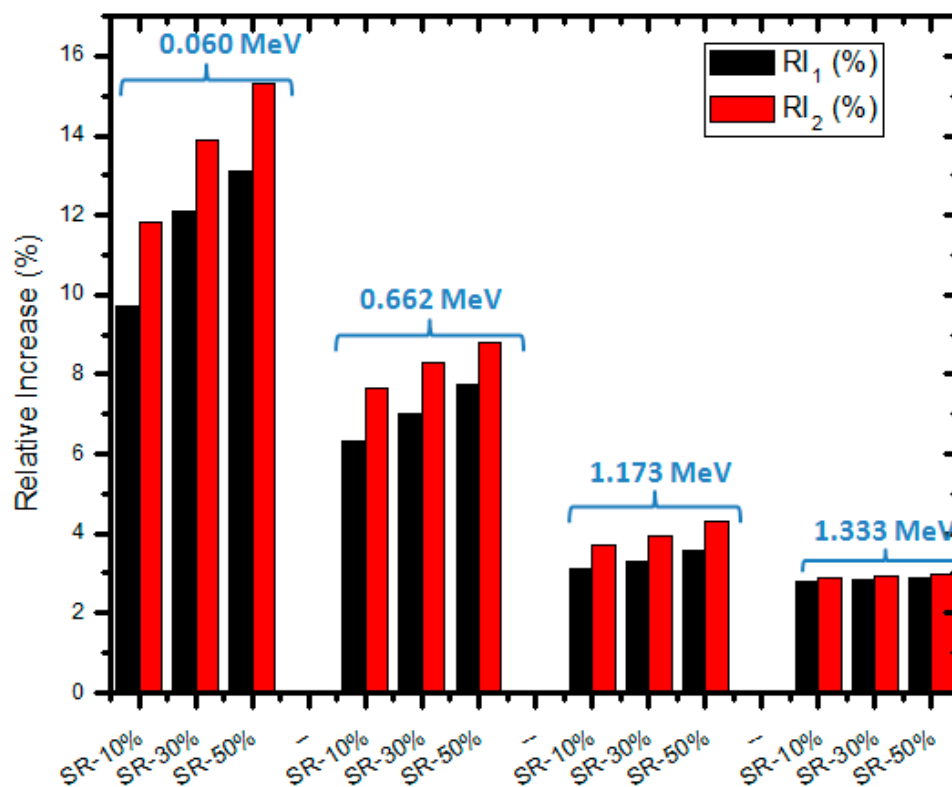


Figure 6. The relative increase between micro and nano as well as micro and 0.5 micro + 0.5 nano CeO₂ at different energies.

The half value layers (HVL) of the SR with micro and nano CeO₂ and the SR with CeO₂ in both sizes (i.e., 0.5 M–0.5 N) at the examined energies were plotted in Figure 7. We observed that the HVL values of the SR with CeO₂ were smaller than those of pure SR when comparing the HVL for the SR with micro and nano, indicating that the addition of CeO₂ to the SR results in superior attenuation. The SR with 10% micro CeO₂ has a greater HVL than the SR with 10% nano CeO₂, as seen in Figure 6. In the meantime, SR with 30% micro CeO₂ had a greater HVL than SR with 30% nano CeO₂. This is due to the fact that the LAC for the SR with nano is higher than that of SR with micro CeO₂ and it is known that the HVL has an inverse relation with the LAC according to the basic formula ($HVL = 0.693/LAC$). The same results are also correct for the SR with 50% CeO₂. This finding demonstrated that the SR containing nanoparticles had a higher attenuation effectiveness than the SR

with micro CeO_2 . When we compare the HVL of the SR with nano CeO_2 and the HVL of SR with 0.5 M–0.5 N, we found that the HVL of the SR containing both sizes (micro and nano) is lower than the HVL of the SR with nano CeO_2 . For example, the HVL for SR with 10% nano CeO_2 at 0.059 MeV is 0.443 cm, while it is 0.434 cm for the SR with 5% micro and 5% nano CeO_2 . For these two samples, the HVL at 0.662 MeV is 3.622 and 3.355 cm. This again confirms the importance of using both micro- and nano-sized CeO_2 in the SR in order to improve the radiation shielding performance. Additionally, it is possible to note from Figure 7 that as the energy increases, the HVL increases for the pure SR in addition to the SR with micro CeO_2 and nano CeO_2 ; consequently, a thicker absorber is desirable in order to reduce the intensity of the radiation by half.

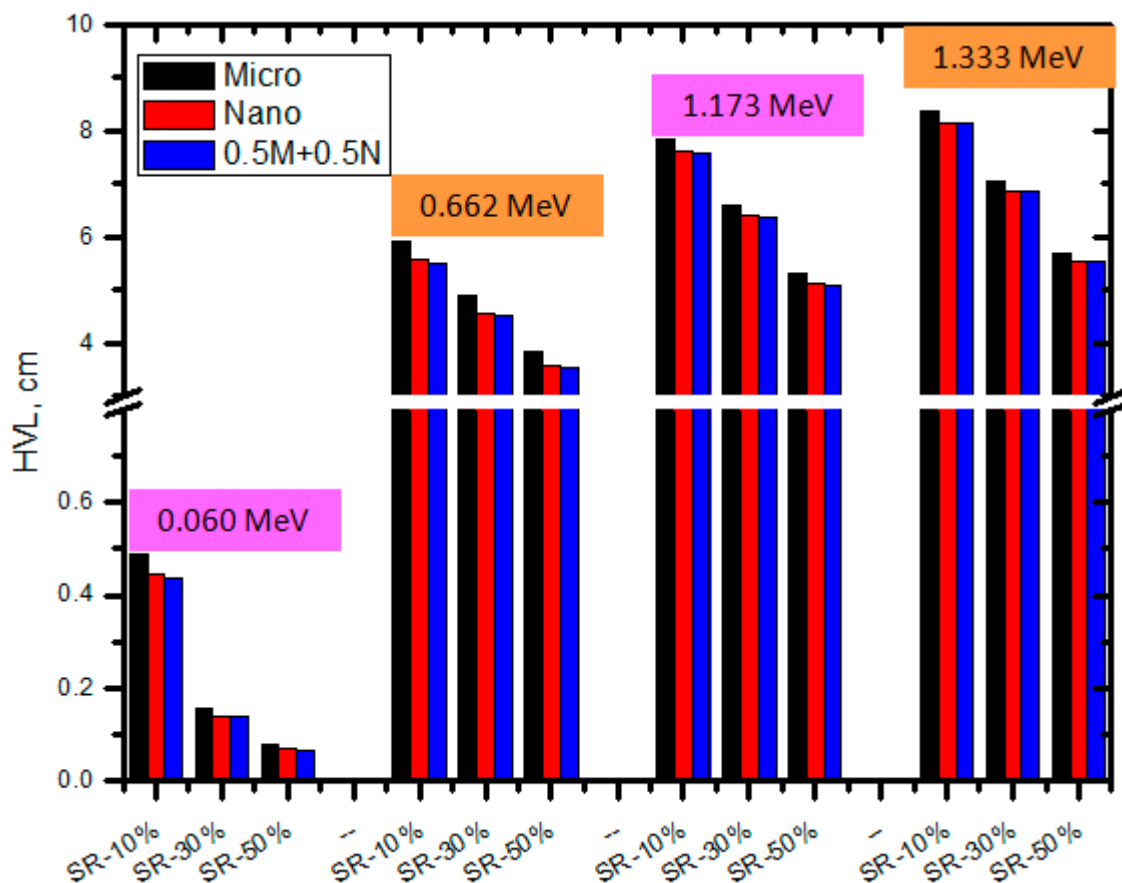


Figure 7. The HVL of SR with micro and nano CeO_2 and the SR with CeO_2 in both sizes at different energies.

Figure 8 displays, in a manner analogous to that of HVL, the 10th value layer (TVL) for the pure SR and the SR containing micro and nano CeO_2 , respectively. The TVL declined when CeO_2 content was increased, as was expected, giving pure SR the highest TVL. Given that Ce is known to have a high atomic number, an increase in the likelihood of interactions between photons and the Ce atom could provide a reasonable interpretation for this tendency. The TVL values of the SR that contains nano CeO_2 were lower than those containing micro CeO_2 according to the analysis of the TVL for the SR doped with micro and nano CeO_2 . As a result, nano CeO_2 is an effective photon shield. The HVL results and this outcome are consistent. These findings suggest that adding nano CeO_2 to the SR significantly improves its shielding characteristics compared to using micro CeO_2 . When comparing the TVL for the SR with only nanoparticles and the SR with both micro and nanoparticles (i.e., 0.5 M–0.5 N), we found that the samples containing both sizes have a lower TVL than the SR with only nanoparticles. For example, the TVL for SR-10% nano CeO_2 is 12.03 cm at 0.662 MeV, and it is 11.14 cm for the SR with 5% micro and 5% nano

CeO₂. It is clear from Figure 7 that the TVL is influenced by the energy of the radiation. Numerically, for the SR with 30% micro CeO₂, the TVL increases from 1.61 to 19.65 cm between 0.059 and 0.662 MeV. We noticed the high difference in the TVL for the same sample between low energy (i.e., 0.059 MeV) and moderate energy (i.e., 0.662 MeV). For this composition, the maximum TVL is 27.85 cm, which was reported at 1.333 MeV.

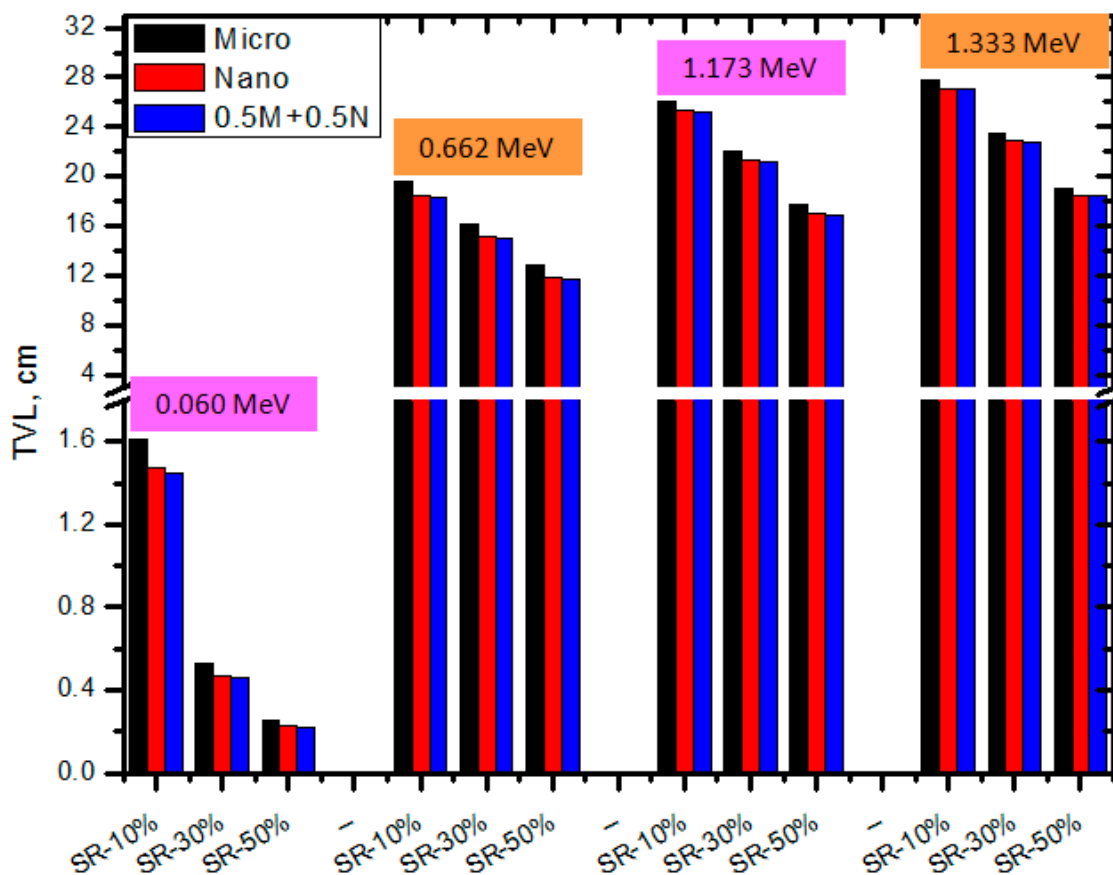


Figure 8. The TVL of SR with micro and nano CeO₂ and the SR with CeO₂ in both sizes at different energies.

Another advantageous parameter is the RPE. This gives explicit information about the efficacy of the particle size, which depends on the RPE of the manufactured SR. The findings of the RSE were presented in Figure 8 for the SR samples that had thicknesses of 2 cm. According to this statistic, pure SR has a lower RPE than any SR that contains micro or nano CeO₂. This result indicates that integrating CeO₂ into SR is a significant way to improve the shielding efficiency of the SR samples. This is due to the fact that Ce is a heavy element, and the addition of CeO₂ to the SR will increase the likelihood that interactions will take place. In addition, looking at Figure 9 reveals that the RPE of the SR treated with nanoparticles is more than that of the SR treated with micro particles when both treatments were given at the same weight fraction. For example, at 0.059 MeV, the RPEs for the SR with 10% micro and nano CeO₂ are 94.2 and 95.6%, respectively, while they are 20.9 and 31.8% for the same samples at 0.662 MeV. This result once again indicates the fact that the attenuation ability is improved when utilizing the nano CeO₂ as opposed to the micro CeO₂. In addition, the findings demonstrated that the SR samples exhibit their highest level of attenuation at 0.059 MeV. The RPE is almost 100% at 0.059 MeV, which means that the SR samples with micro or nano CeO₂ can attenuate almost all the radiation with an energy of 0.059 MeV. The RPE at 0.662 MeV decreases 20–30% for the SR with micro CeO₂, 31–47% for the SR with nano CeO₂, and 34–49% for the samples with both micro and nano CeO₂.

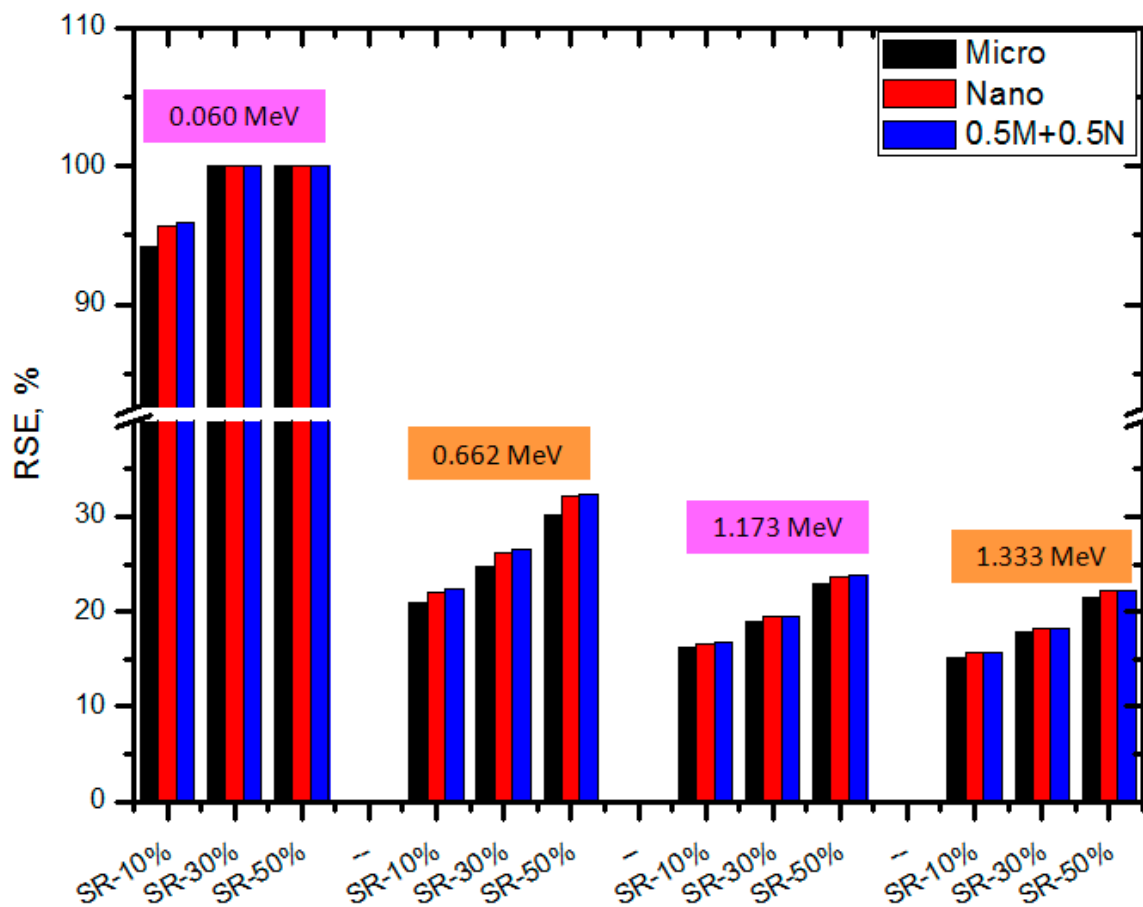


Figure 9. The RPE of SR with micro and nano CeO₂ and the SR with CeO₂ in both sizes at different energies.

4. Conclusions

Research was conducted on the gamma-ray shielding capabilities of SR with micro and nano CeO₂. The experimental approach was employed to find the LAC for each of the SR samples, and the results obtained from the SR containing micro CeO₂ and the Phy-X software were completely consistent with each other. This suggests that the experimental nanoparticle findings were accurate. According to the findings, the LAC values for the nano CeO₂ were greater than those for the micro CeO₂ because the nano CeO₂ had superior particle distribution in the SR. The nanoparticles' lower size enables a more uniform distribution of the particles within the SR, increasing the surface to mass ratio and raising the likelihood of contact between the gamma rays and the nano CeO₂. In addition, calculations were performed for shielding characteristics such as HVL and RPE. According to the findings, the HVL increases as the energy increases from 0.059 to 1.333 MeV for both pure SR and the SR samples with micro and nano CeO₂. This suggests that an SR with a greater thickness is necessary in order to weaken photons with a high level of energy. The RPE results demonstrated that integrating CeO₂ into SR is a significant way for improving the shielding efficiency of the produced SR samples. The RPE results revealed that the RPE of the SR treated with nanoparticles is greater than that of the SR treated with micro particles.

Author Contributions: Conceptualization, M.E.; methodology, M.E.; software, H.M.A. and M.I.A.; formal analysis, H.M.A.; investigation, H.M.A. and W.M.A.-S.; resources, H.M.A.; data curation, W.M.A.-S.; writing—original draft, W.M.A.-S. and M.I.A.; writing—review and editing, M.E. and M.I.A.; visualization, M.E.; supervision, M.E. and M.I.A.; funding acquisition, W.M.A.-S. All authors have read and agreed to the published version of the manuscript.

Funding: This research received no external funding.

Institutional Review Board Statement: Not applicable.

Data Availability Statement: All relevant data are within this paper.

Conflicts of Interest: The authors declare no conflict of interest.

References

1. Chaiphaksa, W.; Borisut, P.; Chanthima, N.; Kaewkhao, J.; Sanwanate, N. Mathematical calculation of gamma rays interaction in bismuth gadolinium silicate glass using WinXCom program. *Mater. Today Proc.* **2022**, *65*, 2412–2415. [[CrossRef](#)]
2. Bagheri, R.; Moghaddam, A.K.; Yousefnia, H. Gamma Ray Shielding Study of Barium-Bismuth-Borosilicate Glasses as Transparent Shielding Materials using MCNP-4C Code, XCOM Program, and Available Experimental Data. *Nucl. Eng. Technol.* **2017**, *49*, 216–223. [[CrossRef](#)]
3. Bilici, S.; Kamislioglu, M.; Guclu, E.E.A. A Monte Carlo simulation study on the evaluation of radiation protection properties of spectacle lens materials. *Eur. Phys. J. Plus* **2023**, *138*, 80. [[CrossRef](#)] [[PubMed](#)]
4. Demir, I.; Gümüş, M.; Gökçe, H.S. Gamma ray and neutron shielding characteristics of polypropylene fiber-reinforced heavy-weight concrete exposed to high temperatures. *Constr. Build. Mater.* **2020**, *257*, 119596. [[CrossRef](#)]
5. Lee, S.Y.; Daugherty, A.M.; Broton, D.J. Assessing aggregates for radiation shielding concrete. *Concr. Int.* **2013**, *35*, 31–38.
6. Aktas, B.; Acikgoz, A.; Yilmaz, D.; Yalcin, S.; Dogru, K.; Yorulmaz, N. The role of TeO₂ insertion on the radiation shielding, structural and physical properties of borosilicate glasses. *J. Nucl. Mater.* **2022**, *563*, 153619. [[CrossRef](#)]
7. Fidan, M.; Acikgoz, A.; Demircan, G.; Yilmaz, D.; Aktas, B. Optical, structural, physical, and nuclear shielding properties, and albedo parameters of TeO₂-BaO-B₂O₃-PbO-V₂O₅ glasses. *J. Phys. Chem. Solids* **2022**, *163*, 110543. [[CrossRef](#)]
8. Sharma, A.; Sayyed, M.; Agar, O.; Tekin, H. Simulation of shielding parameters for TeO₂-WO₃-GeO₂ glasses using FLUKA code. *Results Phys.* **2019**, *13*, 102199. [[CrossRef](#)]
9. Sayyed, M.; Mhareb, M.; Alajerami, Y.; Mahmoud, K.; Imheidat, M.A.; Alshahri, F.; Alqahtani, M.; Al-Abdullah, T. Optical and radiation shielding features for a new series of borate glass samples. *Optik* **2021**, *239*, 166790. [[CrossRef](#)]
10. Yasmin, S.; Kamislioglu, M.; Sayyed, M.I. Assessment of radiation shielding performance of Li₂O-BaO-Bi₂O₃-P₂O₅ glass systems within the energy range from 0.081 MeV to 1.332 MeV via MCNP6 code. *Optik* **2023**, *274*, 170529. [[CrossRef](#)]
11. Kamislioglu, M. An investigation into gamma radiation shielding parameters of the (Al:Si) and (Al+Na):Si-doped international simple glasses (ISG) used in nuclear waste management, deploying Phy-X/PSD and SRIM software. *J. Mater. Sci. Mater. Electron.* **2021**, *32*, 12690–12704. [[CrossRef](#)]
12. Yonphan, S.; Chaiphaksa, W.; Kalkornsurapranee, E.; Tuljitrarn, A.; Kothan, S.; Kaewjaeng, S.; Intachai, N.; Wongdamnern, N.; Kedkaew, C.; Kim, H.; et al. Development of flexible radiation shielding materials from natural Rubber/Sb₂O₃ composites. *Radiat. Phys. Chem.* **2022**, *200*, 110379. [[CrossRef](#)]
13. Aldhuhaihat, M.J.; Amana, M.S.; Jubier, N.J.; Salim, A. Improved gamma radiation shielding traits of epoxy composites: Evaluation of mass attenuation coefficient, effective atomic and electron number. *Radiat. Phys. Chem.* **2021**, *179*, 109183. [[CrossRef](#)]
14. Li, R.; Gu, Y.; Zhang, G.; Yang, Z.; Li, M.; Zhang, Z. Radiation shielding property of structural polymer composite: Continuous basalt fiber reinforced epoxy matrix composite containing erbium oxide. *Compos. Sci. Technol.* **2017**, *143*, 67–74. [[CrossRef](#)]
15. Hosseini, S.H. Study on hard X-ray absorbing properties of nanocluster polyaniline. *Mater. Sci. Semicond. Process.* **2015**, *39*, 90–95. [[CrossRef](#)]
16. Zhang, T.; Li, Y.; Yuan, Y.; Cui, K.; Wei, W.; Wu, J.; Qin, W.; Wu, X. Spatially confined Bi₂O₃-Ti₃C₂Tx hybrids reinforced epoxy composites for gamma radiation shielding. *Compos. Commun.* **2022**, *34*, 101252. [[CrossRef](#)]
17. Sayyed, M.I.; Al-Ghamdi, H.; Almuqrin, A.H.; Yasmin, S.; Elsafi, M. A Study on the Gamma Radiation Protection Effectiveness of Nano/Micro-MgO-Reinforced Novel Silicon Rubber for Medical Applications. *Polymers* **2022**, *14*, 2867. [[CrossRef](#)]
18. Sayyed, M.I.; Yasmin, S.; Almousa, N.; Elsafi, M. The Radiation Shielding Performance of Polyester with TeO₂ and B₂O₃. *Processes* **2022**, *10*, 1725. [[CrossRef](#)]
19. Ambika, M.R.; Nagaiah, N.; Harish, V.; Lokanath, N.K.; Sridhar, M.A.; Renukappa, N.M.; Suman, S.K. Preparation and characterisation of Isophthalic-Bi₂O₃ polymer composite gamma radiation shields. *Radiat. Phys. Chem.* **2017**, *130*, 351–358. [[CrossRef](#)]
20. Kim, S.; Ahn, Y.; Song, S.H.; Lee, D. Tungsten nanoparticle anchoring on boron nitride nanosheet-based polymer nanocomposites for complex radiation shielding. *Compos. Sci. Technol.* **2022**, *221*, 109353. [[CrossRef](#)]
21. Özdemir, T.; Güngör, A.; Akbay, I.; Uzun, H.; Babuçuoğlu, Y. Nano lead oxide and epdm composite for development of polymer based radiation shielding material: Gamma irradiation and attenuation tests. *Radiat. Phys. Chem.* **2018**, *144*, 248–255. [[CrossRef](#)]
22. Prasad, R.; Pai, A.R.; Oyadiji, S.O.; Thomas, S.; Parashar, S. Utilization of hazardous red mud in silicone rubber/MWCNT nanocomposites for high performance electromagnetic interference shielding. *J. Clean. Prod.* **2022**, *377*, 134290. [[CrossRef](#)]
23. Karabul, Y.; İçelli, O. The assessment of usage of epoxy based micro and nano-structured composites enriched with Bi₂O₃ and WO₃ particles for radiation shielding. *Results Phys.* **2021**, *26*, 104423. [[CrossRef](#)]

24. Kaewjaeng, S.; Boonpa, W.; Kothan, S.; Kim, H.; Jumpee, C.; Rajaramakrishna, R.; Tungjai, M.; Kaewkhao, J. X-ray radiation shielding of CeO₂ doped borosilicate glasses and their luminescence characteristics. *Radiat. Phys. Chem.* **2022**, *191*, 109825. [[CrossRef](#)]
25. Kozlovskiy, A.L.; Zdorovets, M.V. Effect of doping of Ce⁴⁺/³⁺ on optical, strength and shielding properties of (0.5 – x)TeO₂-0.25MoO-0.25Bi₂O₃-xCeO₂ glasses. *Mater. Chem. Phys.* **2021**, *263*, 124444. [[CrossRef](#)]
26. Sayyed, M.I.; Hashim, S.; Hannachi, E.; Slimani, Y.; Elsafi, M. Effect of WO₃ Nanoparticles on the Radiative Attenuation Properties of SrTiO₃ Perovskite Ceramic. *Crystals* **2022**, *12*, 1602. [[CrossRef](#)]
27. Sayyed, M.I.; Almurayshid, M.; Almasoud, F.I.; Alyahyawi, A.R.; Yasmin, S.; Elsafi, M. Developed a New Radiation Shielding Absorber Composed of Waste Marble, Polyester, PbCO₃, and CdO to Reduce Waste Marble Considering Environmental Safety. *Materials* **2022**, *15*, 8371. [[CrossRef](#)]
28. D'Souza, A.N.; Padasale, B.; Murari, M.; Karunakara, N.; Sayyed, M.; Elsafi, M.; Al-Ghamdi, H.; Almuqrin, A.H.; Kamath, S.D. TeO₂ for enhancing structural, mechanical, optical, gamma and neutron radiation shielding performance of bismuth borosilicate glasses. *Mater. Chem. Phys.* **2023**, *293*, 126657. [[CrossRef](#)]
29. Hannachi, E.; Sayyed, M.; Slimani, Y.; Elsafi, M. Structural, optical and radiation shielding peculiarities of strontium titanate ceramics mixed with tungsten nanowires: An experimental study. *Opt. Mater.* **2023**, *135*, 113317. [[CrossRef](#)]
30. Şakar, E.; Özpölat, F.; Alm, B.; Sayyed, M.; Kurudirek, M. Phy-X/PSD: Development of a user friendly online software for calculation of parameters relevant to radiation shielding and dosimetry. *Radiat. Phys. Chem.* **2020**, *166*, 108496. [[CrossRef](#)]
31. Hannachi, E.; Sayyed, M.; Slimani, Y.; Almessiere, M.; Baykal, A.; Elsafi, M. Structure and radiation-shielding characteristics of BTO/MnZnFeO ceramic composites. *J. Phys. Chem. Solids* **2023**, *174*, 111132. [[CrossRef](#)]
32. Almuqrin, A.H.; Elsafi, M.; Yasmin, S.; Sayyed, M.I. Morphological and Gamma-Ray Attenuation Properties of High-Density Polyethylene Containing Bismuth Oxide. *Materials* **2022**, *15*, 6410. [[CrossRef](#)]
33. Cheewasukhanont, W.; Limkitjaroenporn, P.; Kothan, S.; Kedkaew, C.; Kaewkhao, J. The effect of particle size on radiation shielding properties for bismuth borosilicate glass. *Radiat. Phys. Chem.* **2020**, *172*, 108791. [[CrossRef](#)]

Disclaimer/Publisher's Note: The statements, opinions and data contained in all publications are solely those of the individual author(s) and contributor(s) and not of MDPI and/or the editor(s). MDPI and/or the editor(s) disclaim responsibility for any injury to people or property resulting from any ideas, methods, instructions or products referred to in the content.